

RESEARCH ARTICLE

# 3D-Printed scaffolds based on poly(Trimethylene carbonate), poly( $\epsilon$ -Caprolactone), and $\beta$ -Tricalcium phosphate

Si-Yao Zheng<sup>1†</sup>, Zhi-Wei Liu<sup>1†</sup>, Hong-Lei Kang<sup>2</sup>, Fan Liu<sup>1\*</sup>, Guo-Ping Yan<sup>1\*</sup>, Feng Li<sup>2</sup>

<sup>1</sup>School of Materials Science and Engineering, Wuhan Institute of Technology, Wuhan 430 205, China

<sup>2</sup>Department of Orthopaedics, Tongji Hospital, Tongji Medical College, Huazhong University of Science and Technology, Wuhan 430 022, China

## Abstract

Three-dimensional (3D)-printed scaffolds of biodegradable polymers have been increasingly applied in bone repair and regeneration, which helps avoid the second surgery. PTMC/PCL/TCP composites were made using poly(trimethylene carbonate), poly( $\epsilon$ -caprolactone), and  $\beta$ -tricalcium phosphate. PTMC/PCL/TCP scaffolds were manufactured using a biological 3D printing technique. Furthermore, the properties of PTMC/PCL/TCP scaffolds, such as biodegradation, mechanic properties, drug release, cell cytotoxicity, cell proliferation, and bone repairing capacity, were evaluated. We showed that PTMC/PCL/TCP scaffolds had low cytotoxicity and good biocompatibility, and they also enhanced the proliferation of osteoblast MC3T3-E1 and rBMSC cell lines, which demonstrated improved adhesion, penetration, and proliferation. Moreover, PTMC/PCL/TCP scaffolds can enhance bone induction and regeneration, indicating that they can be used to repair bone defects *in vivo*.

**Keywords:** Biodegradability; Bone regeneration; Cell proliferation; Poly(trimethylene carbonate); Poly( $\epsilon$ -caprolactone);  $\beta$ -tricalcium phosphate.

<sup>†</sup>These authors contributed equally to this work.

**\*Corresponding author:**

Fan Liu  
(5245934@163.com)  
Guo-Ping Yan  
(guopyan2006@163.com)

**Citation:** Zheng SY, Liu ZW, Kang HL, *et al.*, 2023, 3D-Printed scaffolds based on poly(Trimethylene Carbonate), poly( $\epsilon$ -Caprolactone), and  $\beta$ -Tricalcium phosphate, *Int J Bioprint*, 9(1): 641.  
<https://doi.org/10.18063/ijb.v9i1.641>

**Received:** May 8, 2022

**Accepted:** July 13, 2022

**Published Online:** November 14, 2022

**Copyright:** © 2022 Author(s). This is an Open Access article distributed under the terms of the Creative Commons Attribution License, permitting distribution, and reproduction in any medium, provided the original work is properly cited.

**Publisher's Note:** Whioce Publishing remains neutral with regard to jurisdictional claims in published maps and institutional affiliations.

## 1. Introduction

In recent years, three-dimensional (3D)-printed scaffolds of biomaterials have been increasingly applied for bone regeneration and repairing of bone defects due to the advantage of individual structures<sup>[1-3]</sup>. The ideal biomaterials for bone regeneration scaffolds should have the characteristics, including good biocompatibility, good biodegradability, low toxicity, good mechanical properties, and ease of shaping and disinfection. Moreover, they should have appropriate porosity and pore size to provide a good environment for the growth of new bone tissue, and should have good bone conduction to form autogenous bone instead of substitutes<sup>[4-7]</sup>.

Biodegradable polymeric scaffolds can create the microenvironment and pore network milieu for cell adhesion and bone regeneration, allowing bone defects to be repaired without the need for the second surgery. Poly( $\epsilon$ -caprolactone) (PCL)<sup>[8,9]</sup>,

poly(trimethyl carbonate) (PTMC),<sup>[10,11]</sup> and poly(lactic acid) (PLA)<sup>[12-14]</sup> are some of the appealing biodegradable materials, which are exploited as the carriers for bioengineering and medication delivery. Due to its considerable biodegradability, biocompatibility, and mechanical property, PCL is suitable to be used for making biodegradable scaffolds for bone tissue engineering with minimal inflammatory impact of degradation compounds. However, PCL appears to be hard and have the bulk degradability, high hydrophobicity, and crisp characteristics<sup>[15-17]</sup>. Meanwhile, PTMC has good flexibility, good biocompatibility and biodegradability, low toxicity, and surface corrosion property. Therefore, it is one of the preferred synthetic thermoplastic biomedical polymers for manufacturing in the scaffold for bone regeneration. However, its weak mechanical strength generally hampers its wide application<sup>[18,19]</sup>. PTMC possesses certain good properties that can complement and overcome the disadvantages of PCL to improve the overall flexibility and degradation of the scaffolds.

$\beta$ -Tricalcium phosphate (TCP) has been applied as an ideal bone guide material in orthopedics, spine, plastic surgery, and other fields. Its properties, such as good biocompatibility and biodegradation, excellent safety, and bone-guided regeneration ability, have been recognized by medical practitioners. TCP interacts with osteoblasts and is catabolized to participate in the construction of new bone through humoral dissolution and cell degradation after the implantation *in vivo*. Moreover, its other byproducts can enter the bloodstream and can be metabolized and expelled out of the body; therefore, it will not cause any damages to organs or tissues and give rise to pathological calcification<sup>[20-24]</sup>.

The polymeric composites with nanoceramics offer more mechanical qualities due to the dispersion of nanoparticles in polymer matrix<sup>[25,26]</sup>. In this study, PCL was chosen as a hard polymer matrix and further modified by PTMC, which acted as a soft polymer plasticizer, while TCP nanomaterials were used as reinforcing fillers and bone regeneration inducer. PTMC/PCL/TCP composites in the present study were made of PTMC, PCL, and TCP. Following that, biodegradable PTMC/PCL/TCP scaffolds were created by utilizing biological 3D printing approach, and their qualities in bone implantation applications were also investigated.

## 2. Materials and methods

### 2.1. Preparation of PTMC/PCL/TCP scaffolds

PTMC/TCP composites were made of PTMC (100 – 75% mass) and TCP (0 – 25% mass), and PCL/TCP composites were made of PCL (100 – 75% mass) and TCP

(0 – 25% mass). PTMC/PCL/TCP composites were made of PTMC (50 – 37.5% mass), PCL (50 – 37.5% mass), and TCP (0 – 25% mass)<sup>[27-30]</sup>. PTMC, PCL, and TCP were mixed in dichloromethane and stirred to ensure that the mixture was uniformly fixed. Subsequently, the mixtures were dried *in vacuo* to produce PCL/TCP, PTMC/TCP, and PTMC/PCL/TCP composites.

PTMC/TCP, PCL/TCP, and PTMC/PCL/TCP scaffolds (diameter [mm]  $\times$  height [mm]: 6  $\times$  2, 10  $\times$  2, and 4  $\times$  6, respectively) were produced using Regenovo 3D Bio-Architect<sup>®</sup> Pro Biological 3D printer, and the above composites are used as the raw materials. The following printing conditions were adopted: Conducted at room temperature; inner diameter of print head  $\geq$  0.41 mm; extrusion pressure at 0.3 MPa; and printing rate at 6 mm/s<sup>[31]</sup>.

### 2.2. Cell viability assay

The osteoblast cell lines, clonal murine cell line of immature osteoblasts derived from mice (MC3T3-E1) and rat bone marrow mesenchymal stem cells (rBMSCs), were provided by the China Center for Type Culture Collection of Wuhan University, China<sup>[29]</sup>. 3D-printed PTMC, PCL, PTMC/TCP, PCL/TCP, and PTMC/PCL/TCP scaffolds (diameter [mm]  $\times$  height [mm]: 6  $\times$  2; different TCP content: 0 – 25%) were sanitized for 1 h with ultraviolet light and fastened in 24-well plate. MC3T3-E1 cells ( $4 \times 10^4$ , 200  $\mu$ L) were seeded onto the scaffolds and cultured in the RPMI-1640 media in an incubator (37°C, 5% CO<sub>2</sub>) for 1 and 3 days before being replaced with fresh growth medium. After that, cell counting kit 8 (CKK-8, 10  $\mu$ L) solution, which was purchased from Solarbio (Beijing, China), was added into each well and incubated for 3 h. The absorbance (OD<sub>450</sub>) was determined using a DG-3022A ELISA-Reader (iMark, BioRad, USA).

### 2.3. Degradation assay

All scaffolds (diameter [mm]  $\times$  height [mm]: 10  $\times$  2) were sealed in a dialysis bag containing phosphate-buffered saline (PBS, 10 mL) and shaken in PBS (pH 7.4, 90 mL) at 37°C. The samples were taken out every month, washed, and dried *in vacuo*. Following that, the samples' molecular weight ( $M_n$ ) was measured by gel permeation chromatography, and the weight loss was determined.

### 2.4. DOX release assay

5-DOX-Incorporated PTMC, PCL, PTMC/TCP, PCL/TCP, and PTMC/PCL/TCP scaffolds were prepared according to protocols described in previously published articles.<sup>[13]</sup> The samples sealed in a dialysis bag with PBS (10 mL) and shaken slowly in PBS (pH 7.4, 90 mL) at 37°C. At different time points, fresh PBS (25 mL) was replaced with dialysis solution (25 mL). The variations of DOX concentrations were analyzed.

## 2.5. *In vitro* biocompatibility assay

3D-printed PTMC, PTMC/TCP, PCL/TCP, and PTMC/PCL/TCP scaffolds with 25% TCP content (diameter [mm] × height [mm]: 6 × 2) were sterilized and placed into the 24-well plate. MC3T3-E1 cells ( $6 \times 10^4$ , 200  $\mu$ L culture medium) were seeded onto the scaffolds and cultured for 1 day. Subsequently, paraformaldehyde (4%, 1 mL) was added for 10 min and washed. The scaffolds were then stained using fluorescein isothiocyanate (FITC)-labeled phalloidin (500 nmol/L, Invitrogen Co., USA) for 30 min and washed. Cells were stained again with 4',6-diamidino-2-phenylindole (100 nmol/L, Invitrogen Co., USA) for 10 min and washed, and the scaffolds were stored or photographed at 4°C. The adhesion and growth of the cells in scaffolds were observed using a fluorescence inverted microscope (IX-70, Olympus Co., Ltd., Japan).

## 2.6. Osteogenic gene expression

rBMSCs (initial density:  $8 \times 10^6$  cells/mL) were cultured in 3D-printed scaffolds for 7 and 14 days. At the indicated time point, RNA was extracted from the cells, and 1 mg of RNA was reverse transcribed into complementary DNA (cDNA). siRNA Transfection Reagent (QIAGEN, Hilden, Germany) was utilized following the manufacturer's protocol. The expression of actin, osteocalcin (*OCN*), alkaline phosphatase activity (*ALP*), runt-related transcription factor 2 (*Runx*), and type I collagen (*Col-1*) were quantified and analyzed in triplicate. The relative expression level of each gene was measured and the expression level of each target gene was normalized to the reference housekeeping gene (*GAPDH*).

## 2.7. *In vivo* implantation of PCL/TCP, PTMC/TCP, and PTMC/PCL/TCP scaffolds

Twenty-four Sprague Dawley (SD) rats (weight:  $200 \pm 20$  g) bearing a circular thighbone defect (diameter [mm]: 4) were divided into four groups. 3D-printed PCL/TCP, PTMC/TCP, and PTMC/PCL/TCP scaffolds with 25% TCP content (diameter [mm] × height [mm]: 4 × 6) were implanted in the thighbone defect of the rats. New bone formation was measured using micro-computed tomography (Skyscan1276 X-Ray Microtomograph, Bruker, Belgium). New bone area and percentage were calculated, and 3D reconstruction of interest was also determined.

# 3. Results and discussion

## 3.1. Production of PTMC/TCP, PCL/TCP, and PTMC/PCL/TCP scaffolds

Biodegradable PCL/TCP, PTMC/TCP, and PTMC/PCL/TCP scaffolds were produced using 3D printing technique

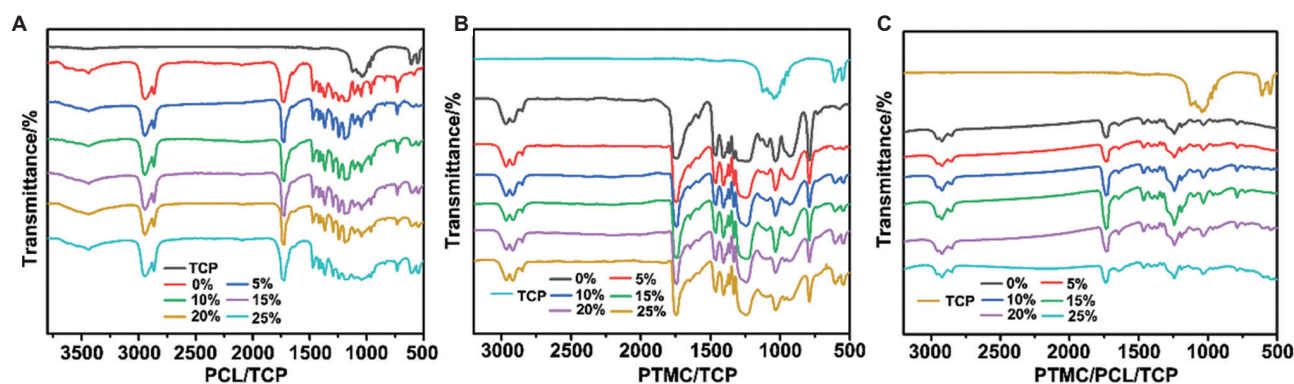
and further characterized. Chemical characterization of PTMC, PCL, TCP, PTMC/TCP, PCL/TCP, and PTMC/PCL/TCP scaffolds was analyzed using Fourier-transform infrared spectroscopy. The spectra of PTMC/TCP displayed characteristic 1740  $\text{cm}^{-1}$  peaks of ester and 2900  $\text{cm}^{-1}$  peaks of CH, and accordingly, peak intensities decreased with increasing of TCP content from 0% to 25% (Figure 1A). Moreover, PTMC/TCP indicated 1040, 960, 603, and 564  $\text{cm}^{-1}$  peaks of P-O and P=O. PCL/TCP also displayed typical 1740  $\text{cm}^{-1}$  peaks of ester, 2900  $\text{cm}^{-1}$  peaks of CH, and 1040, 960, 603, and 564  $\text{cm}^{-1}$  peaks of spectral features of P-O and P=O (Figure 1B). Meanwhile, the spectra of PTMC/PCL/TCP also demonstrated 1948  $\text{cm}^{-1}$  peaks of typical ester, 2960  $\text{cm}^{-1}$  peaks of CH, and accordingly, peak intensities decreased with increasing of TCP content (Figure 1C). Moreover, PTMC/PCL/TCP scaffolds showed P-O and P=O peaks at 1181, 960, 603, and 564  $\text{cm}^{-1}$ .

Figure 2 demonstrates that the water contact angles of all scaffolds increased with TCP content. Moreover, PTMC/PCL/TCP scaffolds showed higher water contact angles than PTMC/TCP scaffolds and lower water contact angles than PCL/TCP scaffolds. This result indicated that PTMC/PCL/TCP scaffolds possessed lower hydrophilicity than PTMC/TCP and higher hydrophilicity than PCL/TCP scaffolds. Therefore, the modification of PCL with PTMC can enhance hydrophilicity of composites.

## 3.2. Scanning electron microscopy of PCL/TCP, PTMC/TCP, and PTMC/PCL/TCP scaffolds

Micrographs of all scaffolds were measured by a scanning electron microscope. Figure 3A-C indicates that TCP scattered uniformly and presented a few aggregations in the scaffolds. The intensity of TCP appeared to increase on the basis of the enlargement of TCP content. Therefore, TCP displayed good compatibility to PTMC and PCL. The micrographs of PTMC/PCL/TCP scaffolds indicate that TCP can enhance the compatibility of PCL and PTMC, in a way similar to the thermals properties above. The phase composition was measured by X-ray diffraction diffractometer (XRD, German Bruker Co., Germany). PCL/TCP, PTMC/TCP, and PTMC/PCL/TCP scaffolds displayed the same typical XRD data as PTMC, PCL, and TCP (Figure 4A-C).

Compressive modulus of scaffolds was determined using MTS universal electronic testing machine according to the standard GB/T 1041-2008; the results are presented in Figure 5A-C and Table 1. All scaffolds showed an increase in compressive modulus with the increase of TCP content. PTMC/PCL/TCP scaffolds displayed higher compressive modulus than PTMC/TCP and lower values



**Figure 1.** Fourier transform infrared of poly( $\epsilon$ -caprolactone) (PCL)/ $\beta$ -tricalcium phosphate (TCP) (A), poly(trimethyl carbonate) (PTMC)/TCP (B), and PTMC/PCL/TCP (C) scaffolds with different TCP content.

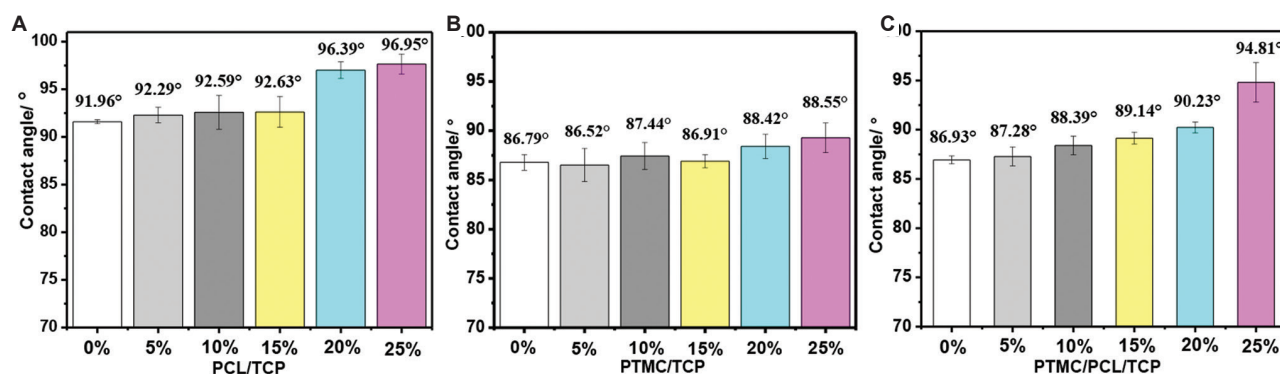


**Figure 2.** Water contact angle of poly( $\epsilon$ -caprolactone) (PCL)/ $\beta$ -tricalcium phosphate (TCP) (A), poly(trimethyl carbonate) (PTMC)/TCP (B), and PTMC/PCL/TCP (C) scaffolds with different TCP content.

than PCL/TCP scaffolds. Compressive moduli of human compact bone and cancellous bone were 14 – 20 GPa and 97.8 – 800 MPa, respectively, while compressive modulus of cartilage was 0.4 – 0.8 MPa<sup>[32,33]</sup>. Therefore, PCL/TCP, PTMC/TCP, and PTMC/PCL/TCP scaffolds displayed lower compressive modulus than human compact bone and obviously higher compressive modulus than cartilage. Moreover, compressive moduli of PCL/TCP and PTMC/PCL/TCP scaffolds were just within the compressive modulus requirements of cancellous bone. Therefore, PCL/TCP and PTMC/PCL/TCP scaffolds are suitable for use in repairing cancellous bone defects. Meanwhile, TCP promoted the compressive property of scaffolds, and the modification of PCL improved the compressive property of PTMC/PCL/TCP scaffolds.

### 3.3. Cell cytotoxicity assay

PCL/TCP, PTMC/TCP, and PTMC/PCL/TCP scaffolds enhanced cell growth of MC3T3-E1 cells (Figure 6). All scaffolds displayed no significant differences in cell proliferation on day 1. PCL/TCP, PTMC/TCP, and PTMC/PCL/TCP scaffolds displayed lower cytotoxicity and higher

proliferation after 3 days of cultivation compared to only 1 day. PTMC/PCL/TCP scaffolds indicated slightly higher cell growth activity than PCL/TCP and PTMC/TCP scaffolds. Thus, PCL/TCP, PTMC/TCP, and PTMC/PCL/TCP exhibited low cytotoxicity, increased the proliferation of MC3T3-E1 cells, and promoted cell growth.

Based on the above measurement, PCL/TCP, PTMC/TCP, and PTMC/PCL/TCP scaffolds with 25% TCP content (PTMC/25%TCP, PCL/25%TCP, and PTMC/PCL/25%TCP) were applied to investigate the degradation, drug-release property, cell proliferation rate, and implantation. Meanwhile, PCL/10%TCP, PTMC/10%TCP, and PTMC/PCL/10%TCP were used as the contrast controlled samples.

### 3.4. Degradation

All scaffolds displayed  $M_n$  loss and weight loss in PBS (Figure 7A and B). PTMC/PCL/TCP scaffolds showed the similar weight loss and  $M_n$  loss pattern as that of PCL/TCP scaffolds after degradation for 6 months. PTMC/25%TCP scaffolds displayed similar low weight

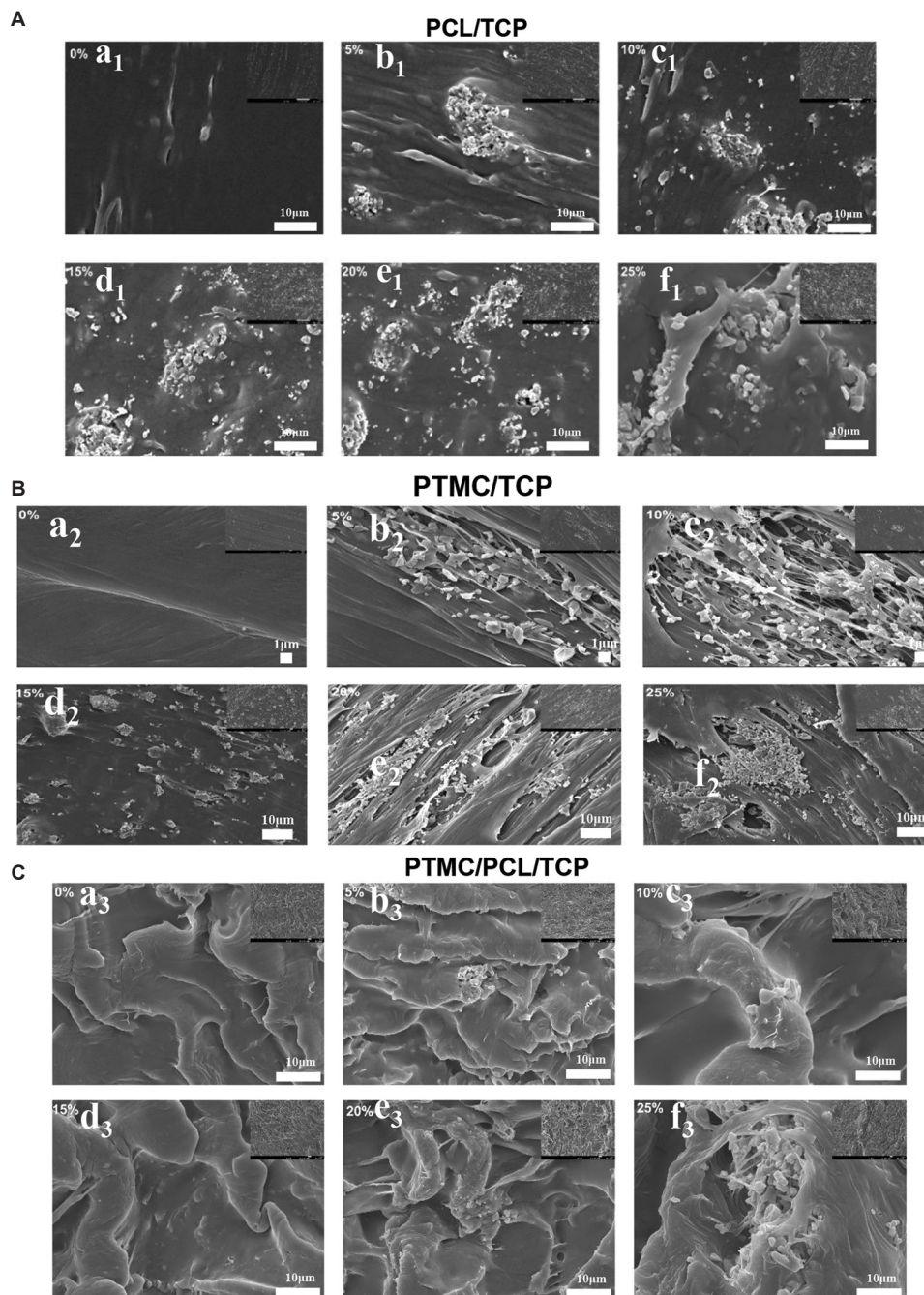


**Figure 3.** The micrographs of (A) poly( $\epsilon$ -caprolactone) (PCL)/ $\beta$ -tricalcium phosphate (TCP), (B) poly(trimethyl carbonate) (PTMC)/TCP, and (C) PTMC/PCL/TCP scaffolds with different TCP content. PTMC/TCP scaffolds with (a<sub>1</sub>) 0%, (b<sub>1</sub>) 5%, (c<sub>1</sub>) 10%, (d<sub>1</sub>) 15%, (e<sub>1</sub>) 20%, and (f<sub>1</sub>) 25% TCP content; PCL/TCP scaffolds with (a<sub>2</sub>) 0%, (b<sub>2</sub>) 5%, (c<sub>2</sub>) 10%, (d<sub>2</sub>) 15%, (e<sub>2</sub>) 20%, and (f<sub>2</sub>) 25% TCP content; PTMC/PCL/TCP scaffolds with (a<sub>3</sub>) 0%, (b<sub>3</sub>) 5%, (c<sub>3</sub>) 10%, (d<sub>3</sub>) 15%, (e<sub>3</sub>) 20%, and (f<sub>3</sub>) 25% TCP content.

loss and higher  $M_n$  loss than PTMC scaffolds. PTMC/PCL/25%TCP underwent higher weight loss and lower  $M_n$  loss than PTMC/PCL scaffolds, while PTMC/PCL/25%TCP showed a slight weight loss compared to PTMC/PCL/10%TCP scaffolds. PCL/10%TCP underwent relatively higher  $M_n$  loss than PCL/25%TCP and PCL

scaffolds. PTMC/PCL/25%TCP had lower  $M_n$  loss than PTMC/PCL/10%TCP and PTMC/PCL scaffolds. Thus, TCP nanoparticles probably induced the occurrence of lower weight loss and higher  $M_n$  loss, increasing of water permeation in composites, and further acceleration of hydrolysis and degradation.

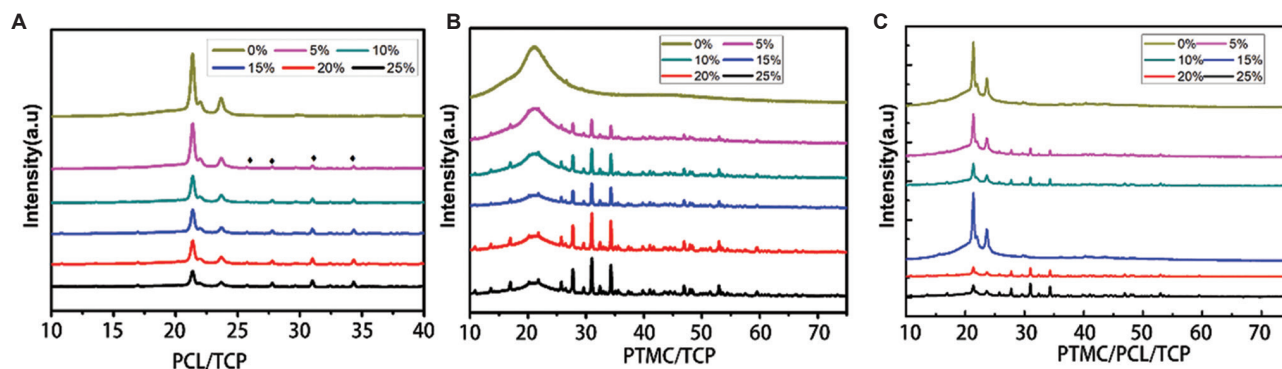


Figure 4. XRD of poly( $\epsilon$ -caprolactone) (PCL)/ $\beta$ -tricalcium phosphate (TCP) (A), poly(trimethyl carbonate) (PTMC)/TCP (B), and PTMC/PCL/TCP (C) scaffolds with different TCP content.

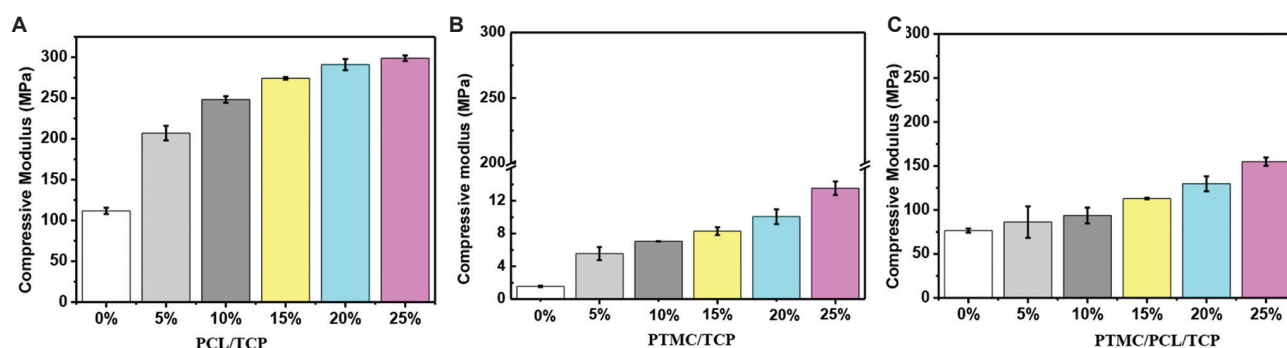


Figure 5. Compressive modulus of poly( $\epsilon$ -caprolactone) (PCL)/ $\beta$ -tricalcium phosphate (TCP) (A), poly(trimethyl carbonate) (PTMC)/TCP (B), and PTMC/PCL/TCP (C) scaffolds with different TCP content.

Table 1. Compressive property of PCL/TCP, PTMC/TCP, and PTMC/PCL/TCP scaffolds

Scaffolds	Compressive modulus (MPa)	F $\sigma$ =50% (N)
PCL	111.8	1157.7
PCL/5%TCP	207.0	2065.8
PCL/10%TCP	248.2	2223.0
PCL/15%TCP	274.1	2423.8
PCL/20%TCP	290.9	2570.1
PCL/25%TCP	298.8	2682.9
PTMC	1.5	81.4
PTMC/5%TCP	5.6	312.8
PTMC/10%TCP	7.1	371.5
PTMC/15%TCP	8.3	241.3
PTMC/20%TCP	10.1	303.1
PTMC/25%TCP	13.5	470.6
PTMC/PCL	76.5	1099.6
PTMC/PCL/5%TCP	86.2	1277.1
PTMC/PCL/10%TCP	93.6	1299.2
PTMC/PCL/15%TCP	113.0	1348.3
PTMC/PCL/20%TCP	129.8	1468.6
PTMC/PCL/25%TCP	154.8	1552.4

PCL: Poly( $\epsilon$ -caprolactone); TCP:  $\beta$ -tricalcium phosphate; PTMC: Poly (trimethyl carbonate)

### 3.5. DOX release property

All scaffolds demonstrated substantial release rates and steady drug controlled release properties during 130 days of measurement (Figure 8). PTMC/TCP scaffolds with different TCP content showed similar DOX release rates. Compared with PTMC/TCP scaffolds, PTMC/PCL/TCP scaffolds displayed faster DOX release rates, presumably due to the large pores of scaffolds and high drug diffusion coefficient. PCL/TCP scaffolds displayed obviously slower release rates because of its low hydrophilicity, slow degradation rate, and low drug diffusion coefficient. Meanwhile, the DOX release rates of scaffolds increased with the increased of TCP content. PTMC/PCL/25%TCP and PTMC/25%TCP displayed 18.1% and 14.1% of cumulative DOX release, respectively, which were higher than PCL/TCP (3.1%). Thus, TCP improved the hydrophilicity, drug diffusion coefficients, and DOX release rates of scaffolds. These results are consistent with the micrographs structures of PCL/TCP, PTMC/TCP, and PTMC/PCL/TCP scaffolds in this study.

### 3.6. In vitro biocompatibility assay

Porous 3D-printed PCL/TCP, PTMC/TCP, and PTMC/PCL/TCP scaffolds can provide a large surface area, which

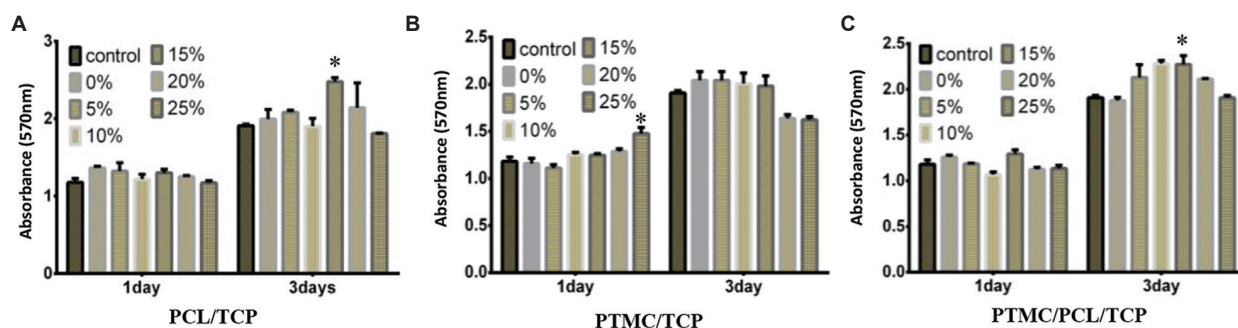


Figure 6. Cell cytotoxicity assays of poly( $\epsilon$ -caprolactone) (PCL)/ $\beta$ -tricalcium phosphate (TCP) (A), poly(trimethyl carbonate) (PTMC) (B)/TCP, and PTMC/PCL/TCP (C) scaffolds with different TCP content to osteoblast MC3T3-E1 cells (\* $P < 0.05$  vs. control).

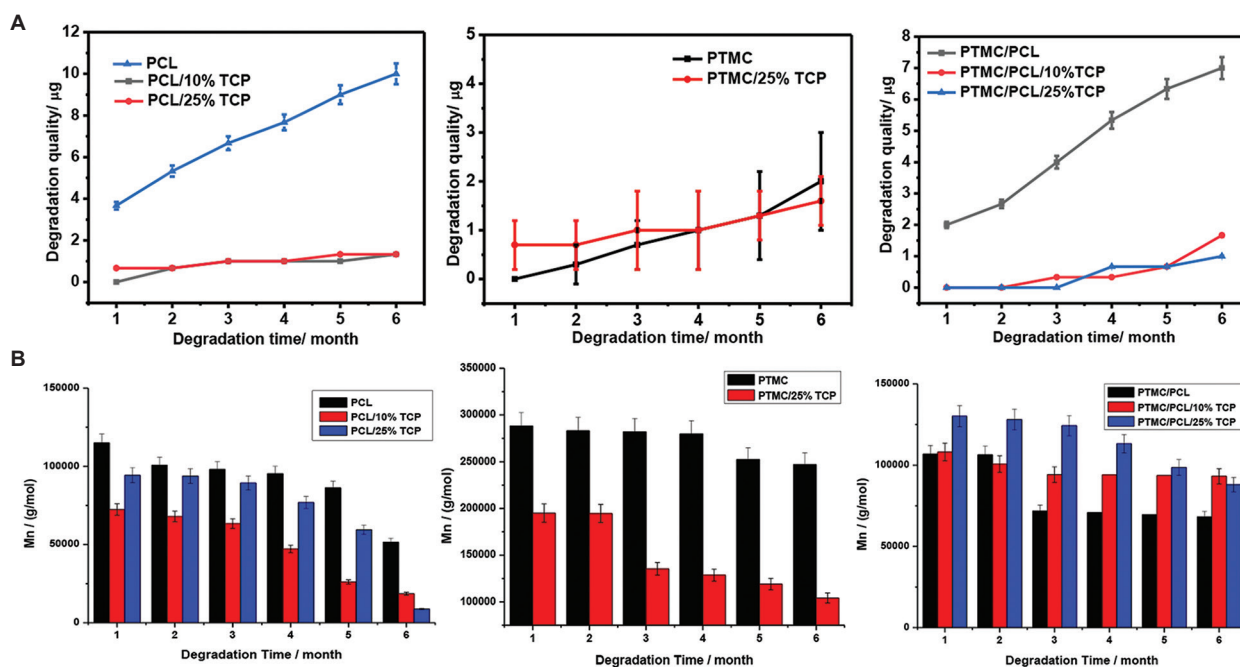


Figure 7. Weight loss (A) and  $M_n$  loss (B) of poly( $\epsilon$ -caprolactone) (PCL)/ $\beta$ -tricalcium phosphate (TCP), poly(trimethyl carbonate) (PTMC)/TCP, and PTMC.

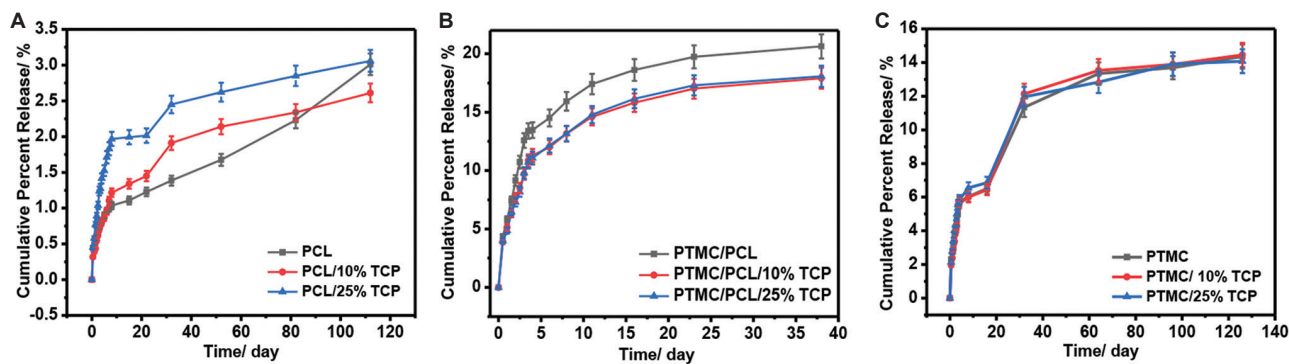
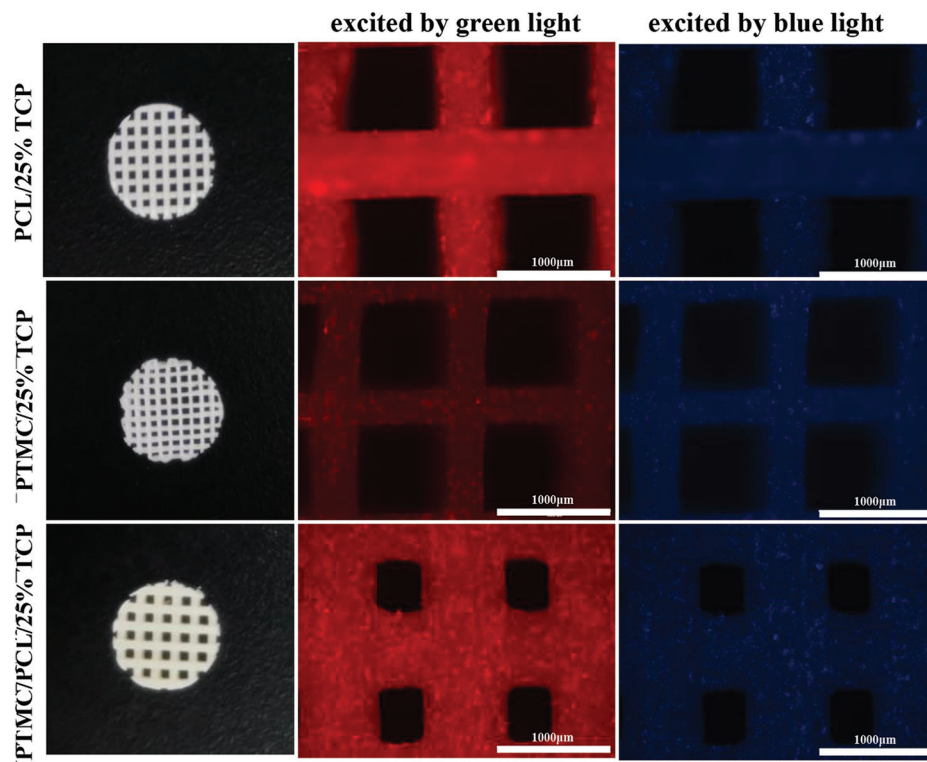
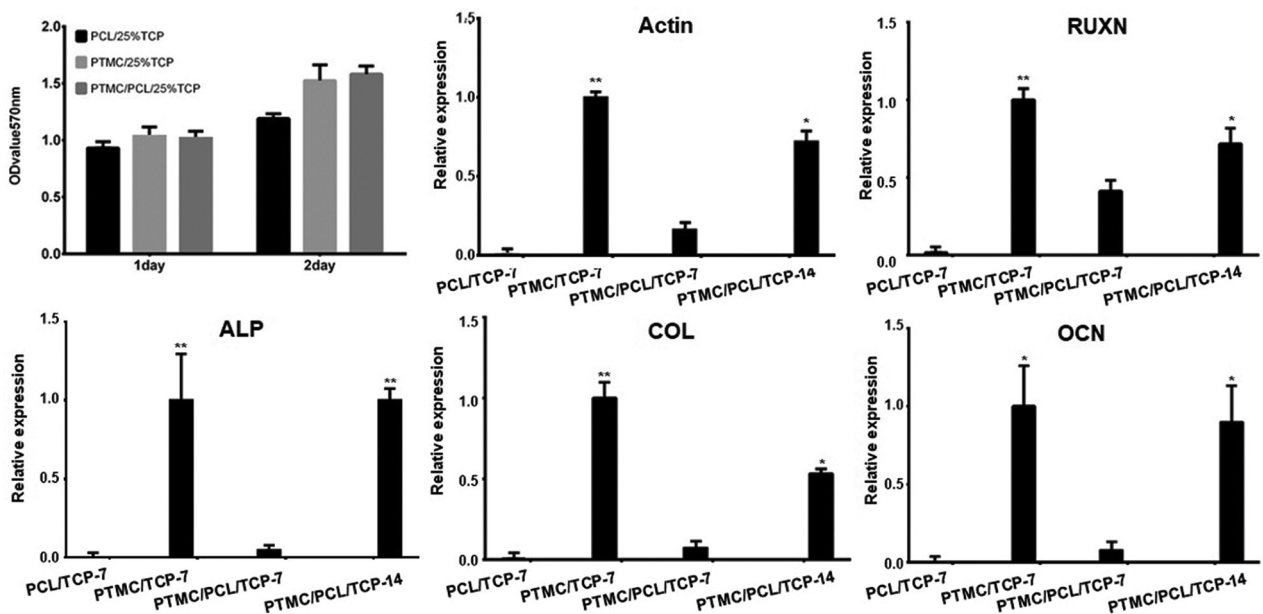


Figure 8. (A-C) Release profiles of DOX from poly( $\epsilon$ -caprolactone) (PCL)/ $\beta$ -tricalcium phosphate (TCP), poly(trimethyl carbonate) (PTMC)/TCP, and PTMC/PCL/TCP scaffolds.



**Figure 9.** Osteoblast MC3T3-E1 cell proliferation assays on poly( $\epsilon$ -caprolactone) (PCL)/ $\beta$ -tricalcium phosphate (TCP), poly(trimethyl carbonate) (PTMC)/TCP, and PTMC/PCL/TCP scaffolds with 25% TCP content.



**Figure 10.** Gene expression assays on rBMSCs in poly( $\epsilon$ -caprolactone) (PCL)/ $\beta$ -tricalcium phosphate (TCP), poly(trimethyl carbonate) (PTMC)/TCP, and PTMC/PCL/TCP scaffolds with 25% TCP content. Abbreviations: PCL/TCP-7, PCL/25%TCP scaffolds for 7 days; PTMC/TCP-7, PTMC/25%TCP scaffolds for 7 days; PTMC/PCL/TCP-7, PTMC/PCL/25%TCP scaffolds for 7 days; and PTMC/PCL/TCP-14, PTMC/PCL/25%TCP scaffolds for 14 days.

is conducive to cell proliferation, differentiation, and metabolism. **Figure 9** indicates that 3D-printed PCL/TCP,

PTMC/TCP, and PTMC/PCL/TCP scaffolds displayed the uniform pore size and micro-network structures.

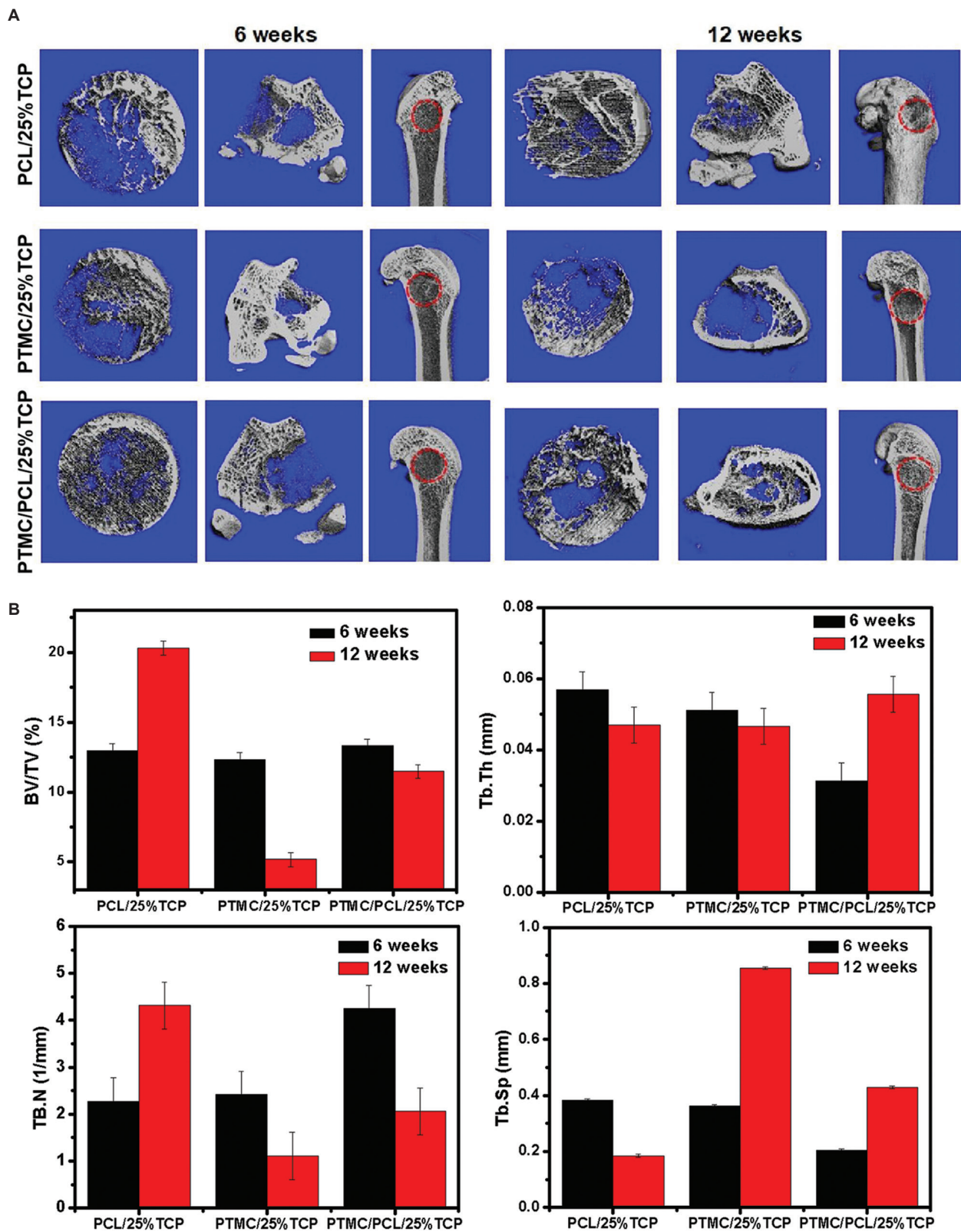


**Figure 11.** Bone repairing assays in thigh bone defect in rats. (A) Micro-CT images of thigh bone defect in rats implanted with poly( $\epsilon$ -caprolactone) (PCL)/25% $\beta$ -tricalcium phosphate (TCP), poly(trimethyl carbonate) (PTMC)/25%TCP, and PTMC/PCL/25%TCP. (B) New formed bone parameters after 6 weeks and 12 weeks of surgery.

Through the porosity test, we found that the porosity of 3D-printed PCL/25%TCP, PTMC/25%TCP, and PTMC/PCL/25%TCP scaffolds was  $66.43 \pm 2.56\%$ ,  $58.9 \pm 2.81\%$ , and  $48.0 \pm 1.84\%$ , respectively.

MC3T3-E1 cells were evenly distributed in 3D-printed PCL/25%TCP, PTMC/25%TCP, and PTMC/PCL/25%TCP scaffolds, which provided microenvironment for cell adhesion and regeneration. MC3T3-E1 cells scattered uniformly, adhered, grew and proliferated in scaffolds, and afterward, the cells synthesized and secreted matrix proteins. MC3T3-E1 cells appeared to have good attachment states and proliferated in PCL/25%TCP, PTMC/25%TCP, and PTMC/PCL/25%TCP scaffolds. TCP also promoted the expression of osteoblast-related genes, alkaline phosphatase gene, and bone adhesion gene, leading to the differentiation of osteoblasts as well as the mineralization and formation of bone. Moreover, the degraded Ca and P from TCP in the body can enter the living circulatory system, which can promote the formation of new bone. PTMC/PCL/25%TCP scaffolds displayed better biocompatibility and stimulated a greater extent of cell regeneration than PTMC/25%TCP and PCL/25%TCP scaffolds.

### 3.7. Osteogenic gene expression

Metabolic activity of rBMSCs was studied after 1 and 2 days of post-culturing in 3D-printed PCL/25%TCP, PTMC/25%TCP, and PTMC/PCL/25%TCP scaffolds. mRNA expression results are presented in Figure 10. Cell proliferation on all scaffolds at 1 day was higher than that at 2 days. Moreover, PTMC/PCL/25%TCP and PTMC/25%TCP scaffolds demonstrated higher levels of cellular metabolic activity than PCL/25%TCP scaffolds at 1 day and 2 days. Meanwhile, PTMC/PCL/25%TCP scaffolds showed slightly higher metabolic activity than PTMC/25%TCP at 2 days.

The PCL/25%TCP, PTMC/25%TCP, and PTMC/PCL/25%TCP scaffolds promoted rBMSCs growth and improved the gene expression of actin, ALP, COL, RUNX2, and OCN. Moreover, rBMSCs scattered uniformly and induced adhesion and regeneration in the scaffolds (Figure 10). PTMC/PCL/25%TCP and PTMC/25%TCP scaffolds evidently enhanced gene expression of actin, ALP, COL, RUNX2, and OCN. However, PCL/25%TCP scaffolds appeared to have almost no gene expression at 7 days post-culturing. Meanwhile, PTMC/25%TCP scaffolds showed higher gene expression than PTMC/PCL/25%TCP scaffolds at 7 days post-culturing. Moreover, PTMC/PCL/25%TCP scaffolds demonstrated higher level of gene expression at 14 days post-culturing than that at 7 days post-culturing. Therefore, PTMC/PCL/25%TCP and PTMC/25%TCP

scaffolds displayed good biocompatibility, high cell proliferation performances, high metabolic activity, and gene expression of actin, ALP, COL, RUNX2, and OCN.

### 3.8. *In vivo* bone regeneration

All scaffolds were embedded in thigh bone defects for 12 weeks. New bone tissue data, including bone tissues volume/total tissue volume (BV/TV, %), trabecular space (Tb.Sp, mm), number of trabecula (Tb.N,  $\text{mm}^{-1}$ ), and trabecular thickness (Tb.Th, mm) were evaluated. As shown in Figure 11A, plenty of new bone tissues were found in thigh defects of the rats and gradually penetrated into either PCL/25%TCP, PTMC/25%TCP, or PTMC/PCL/25%TCP scaffolds after 6 and 12 weeks. Moreover, bone tissues continued growing to form a network, which repaired bone defects in pace with biodegradation of scaffolds. Figure 11B indicates the new formed bone parameters after 6 weeks and 12 weeks of surgery.

More formation of new bones appeared in thigh defects of the rats implanted with PTMC/PCL/25%TCP and PCL/25%TCP scaffolds than in those with PTMC/25%TCP scaffolds after 6 weeks and 12 weeks. The formation of new bone in PCL/25%TCP and PTMC/PCL/25%TCP scaffolds was higher than that in PTMC/25%TCP scaffold. Therefore, PCL/25%TCP and PTMC/PCL/25%TCP scaffolds can display high osteogenic activity, suggesting its role in bone repair.

## 4. Conclusion

3D-printed PCL/TCP, PTMC/TCP, and PTMC/PCL/TCP scaffolds provide good porous growth microenvironments and mechanic supports for MC3T3-E1 cells and rBMSCs, and also enhance the proliferation of osteoblast cells. Moreover, PTMC/PCL/TCP and PCL/TCP scaffolds display good biodegradability, good biocompatibility, and high osteogenic activity, which can be used to repair bone defects *in vivo*.

## Acknowledgments

Not applicable.

## Funding

This work was supported by the Key National Research and Development Program (Grant No. 2018YFB1105502, 2016YFB1101302), Frontier Project of Application Foundation of Wuhan Former Funded Science and Technology Program (Grant No. 2020020601012252), Innovative Talents Project of Yellow Crane Talents Plan of Wuhan City (Grant [2017] No.1), Scientific research projects for high level talents in the new century of Hubei Province (Grant

[2017] No.344), Scientific Research Fund Project of Wuhan Institute of Technology (Grant No. K201861), and South Hubei Talents Project of Innovation and Entrepreneurship (Grant [2019] No.11).

### Conflict of interest

All authors declare that they have no conflicts of interest.

### Author contributions

G-P.Y. designed the experiments. F.L., S-Y.Z., and Z-W.L. manufactured and characterized the samples. H-L.K. and F.L. carried out the *in vitro* and *in vivo* experiments. F.L. and G-P.Y. wrote the paper and conducted the analysis and discussions. All authors discussed the results and commented on the manuscript. S-Y.Z. and Z-W.L. contributed equally to this work.

### Ethics approval and consent to participate

All animal experiments were performed at the Tongji Hospital of Huazhong University of Science and Technology in accordance with protocols approved by the Institutional Animal Care and Use Committee.

### Consent for publication

Not applicable.

### Availability of data

The data that support the findings of this study are available from the corresponding author on reasonable request.

### References

1. Ligon SC, Liska R, Stampfl J, *et al.*, 2017, Polymers for 3D printing and customized additive manufacturing. *Chem Rev*, 117: 10212–10290.  
<https://doi.org/10.1021/acs.chemrev.7b00074>
2. Matai I, Kaur G, Seyedsalehi A, *et al.*, 2020, Progress in 3D bioprinting technology for tissue/organ regenerative engineering. *Biomaterials*, 226: 119536.  
<https://doi.org/10.1016/j.biomaterials.2019.119536>
3. Yan YF, Chen H, Zhang HB, *et al.*, 2019, Vascularized 3D printed scaffolds for promoting bone regeneration. *Biomaterials*, 190–1: 97–110.  
<https://doi.org/10.1016/j.biomaterials.2018.10.033>
4. Liang Q, Ma Y, Yao X, *et al.*, 2022, Advanced 3D-printing bioinks for articular cartilage repair. *Int J Bioprint*, 8: 511.
5. Bunpetch V, Zhang XA, Li T, *et al.*, 2019, Silicate-based bioceramic scaffolds for dual-lineage regeneration of osteochondral defect. *Biomaterials*, 192: 323–333.  
<https://doi.org/10.1016/j.biomaterials.2018.11.025>
6. Zhuang P, Sun AX, An J, *et al.*, 2018, 3D Neural tissue models: from spheroids to bioprinting. *Biomaterials*, 154: 113–133.  
<https://doi.org/10.1016/j.biomaterials.2017.10.002>
7. Daly AC, Pitacco P, Nulty J, *et al.*, 2018, 3D printed microchannel networks to direct vascularisation during endochondral bone repair. *Biomaterials*, 162: 34–46.  
<https://doi.org/10.1016/j.biomaterials.2018.01.057>
8. Liu DH, Nie W, Li DJ, *et al.*, 2019, 3D printed PCL/SrHA scaffold for enhanced bone regeneration. *Chem Eng J*, 362: 269–279.
9. Agudelo RR, Scheuermann K, García AG, *et al.*, 2018, Hybrid nanofibers based on poly-caprolactone/gelatin/hydroxyapatite nanoparticles-loaded doxycycline: effective anti-tumoral and antibacterial activity. *Mat Sci Eng C Mater Biol Appl*, 83: 25–34.  
<https://doi.org/10.1016/j.msec.2017.08.012>
10. Kang HL, Jiang XD, Liu ZW, *et al.*, 2021, Biodegradable 3D printed scaffolds of modified poly (Trimethylene Carbonate) composite materials with poly (L-Lactic Acid) and hydroxyapatite for bone regeneration. *Nanomaterials (Basel)*, 11: 3215.  
<https://doi.org/10.3390/nano11123215>
11. Hu B, Du HJ, Yan GP, *et al.*, 2014, Magnetic polycarbonate microspheres for tumor-targeted delivery of tumor necrosis factor. *Drug Deliv*, 21: 204–212.  
<https://doi.org/10.3109/10717544.2013.843609>
12. Wang X, Jiang M, Zhou ZW, *et al.*, 2017, 3D printing of polymer matrix composites: A review and prospective. *Composites B*, 110: 442–458.  
<https://doi.org/10.1016/j.compositesb.2016.11.034>
13. Han SH, Cha MS, Jin YZ, *et al.*, 2021, BMP-2 and hMSC dual delivery onto 3D printed PLA-biogel scaffold for critical-size bone defect regeneration in rabbit tibia. *Biomed Mater*, 16: 015019.  
<https://doi.org/10.1088/1748-605X/aba879>
14. Aihemaiti P, Jiang H, Aiyiti W, *et al.*, 2022, Optimization of 3D printing parameters of biodegradable polylactic acid/hydroxyapatite composite bone plates. *Int J Bioprint*, 8: 490.  
<https://doi.org/10.18063/ijb.v8i1.490>
15. Lu K, Yan GP, Chen H, *et al.*, 2009, Microwave-assisted ring-opening copolymerization of  $\epsilon$ -caprolactone and 2-phenyl-5,5-bis(oxymethyl) trimethylene carbonate. *Sci Bull*, 54: 3237–3243.
16. Feng TJ, Mei LL, Liu F, *et al.*, 2021, Microwave-assisted ring-opening copolymerization and property of polycarbonates. *Polym Adv Technol*, 32: 3412–3420.
17. Liu H, Wu F, Chen R, *et al.*, 2022, Electrohydrodynamic

- jet-printed ultrathin polycaprolactone scaffolds mimicking bruch's membrane for retinal pigment epithelial tissue engineering. *Int J Bioprint*, 8: 550.
18. Xiong X, Xia J, Shaojie Y, *et al.*, 2021, Solvent evaporation induced fabrication of porous polycaprolactone scaffold via low-temperature 3D printing for regeneration medicine researches. *Polymer*, 217: 123436.  
<https://doi.org/10.1016/j.polymer.2021.123436>
  19. Guney A, Maldo J, Dhert WJA, *et al.*, 2017, Triblock copolymers based on caprolactone and 1,3-trimethylene carbonate for the 3D printing of tissue engineering scaffolds. *Int J Artif Ogran*, 40: 176–184.  
<https://doi.org/10.5301/ijao.5000543>
  20. UIIah I, Cao L, Cui W, *et al.*, 2021, Stereolithography printing of bone scaffolds using biofunctional calcium phosphate nanoparticles. *J Mater Sci Technol*, 88: 99–108.
  21. Chen L, Deng CJ, Li JY, *et al.*, 2019, 3D printing of a lithium-calcium-silicate crystal bioscaffold with dual bioactivities for osteochondral interface reconstruction. *Biomaterials*, 196: 138–150.  
<https://doi.org/10.1016/j.biomaterials.2018.04.005>
  22. Ma HS, Feng C, Chang J, *et al.*, 2018, 3D-printed bioceramic scaffolds: from bone tissue engineering to tumor therapy. *Acta Biomater*, 79: 37–59.  
<https://doi.org/10.1016/j.actbio.2018.08.026>
  23. Li DW, Zhang K, Shi C, *et al.*, 2018, Small molecules modified biomimetic gelatin/hydroxyapatite nanofibers constructing an ideal osteogenic microenvironment with significantly enhanced cranial bone formation. *Int J Nanomedicine*, 13: 7167–7181.  
<https://doi.org/10.2147/IJN.S174553>
  24. Marc B, Le Gars SB, Nicola D, 2020,  $\beta$ -Tricalcium phosphate for bone substitution: Synthesis and properties. *Acta Biomater*, 113: 23–41.  
<https://doi.org/10.1016/j.actbio.2020.06.022>
  25. Jang J, Park JY, Gao G, *et al.*, 2018, Biomaterials-based 3D cell printing for next-generation therapeutics and diagnostics. *Biomaterials*, 156: 88–106.  
<https://doi.org/10.1016/j.biomaterials.2017.11.030>
  26. Corcione CE, Gervaso F, Scalera F, *et al.*, 2019, Highly loaded hydroxyapatite microsphere/pla porous scaffolds obtained by fused deposition modeling. *Ceram Int*, 45: 2803–2810.
  27. Chen H, Yan GP, Li L, *et al.*, 2009, Synthesis, characterization and properties of  $\epsilon$ -caprolactone and carbonate copolymers. *J Appl Polym Sci*, 114: 3087–3096.
  28. Liu F, Mei LL, Tan ZL, *et al.*, 2016, Studies on microwave-assisted ring-opening polymerization and property of poly (9-phenyl-2,4,8,10-tetraoxaspiro-[5,5]undecane-3-one). *Chin. J Polym Sci*, 34: 1330–1338.
  29. Shi FQ, 1990, How to copy the disease model of animals. In: medical animal experiment method. Ch. 4. Beijing, china: people's medical publishing house, p226–232.
  30. Liu F, Kang HL, Liu ZW, *et al.*, 2021, 3D printed multi-functional scaffolds based on poly( $\epsilon$ -caprolactone) and hydroxyapatite composites. *Nanomaterials (Basel)*, 11: 2456.  
<https://doi.org/10.3390/nano11092456>
  31. Liu YQ, Li T, Ma HS, *et al.*, 2018, 3D-printed scaffolds with bioactive elements-induced photothermal effect for bone tumor therapy. *Acta Biomater*, 73: 531–46.  
<https://doi.org/10.1016/j.actbio.2018.04.014>
  32. Morgan EF, Unnikrisnan GU, Hussein AI, 2018, Bone mechanical properties in healthy and diseased states. *Annu Rev Biomed Eng*, 20: 119–143.  
<https://doi.org/10.1146/annurev-bioeng-062117-121139>
  33. Roberts CR, Rains JK, Paré PD, *et al.*, 1997, Ultrastructure and tensile properties of human tracheal cartilage. *J Biomech*, 31: 81–6.  
[https://doi.org/10.1016/s0021-9290\(97\)00112-7](https://doi.org/10.1016/s0021-9290(97)00112-7)